An evaporation test based on thermal infra red remote-sensing to select appropriate soil hydraulic properties

Gilles Boulet, Bernard Mougenot, T. Ben Abdelouahab

An evaporation test based on Thermal Infra Red Remote-Sensing to select appropriate soil hydraulic properties

Gilles Boulet[1], Bernard Mougenot[1] and Tarik Ben Abdelouahab[2]

[1] CESBIO (Université de Toulouse, CNRS, CNES, IRD), 18 Avenue Edouard Belin, bpi 2801, 31401 Toulouse cedex 9, France. Corresponding author : Gilles.Boulet@cesbio.cnes.fr

[2] INRA, Centre Régional de la Recherche Agronomique du Tadla, Domaine Expérimental d'Afourer, B.P. 567 Provincial de Beni-Mellal, Morocco

Abstract

Pedotransfer functions are the most widely used method to estimate common soil hydraulic properties at regional scale. Since they rely on an empirical link between textural and structural soil properties observed in the laboratory on undisturbed soil samples, one must check whether the pedotransfer functions built elsewhere also apply to the location of interest. Alternative methods to laboratory analysis, such as infiltration tests, exist but are difficult to carry out at large scales. Here we propose a method for selecting appropriate soil hydraulic properties based on the physical link between the soil water diffusion properties and the plant water stress, which has been named the "evaporation test". It consists in (i) detecting water stress from remote sensing data in the Thermal Infra Red spectrum and a simulated unstressed surface temperature, then (ii) estimating the date of the last irrigation/rainfall event, the water content at the end of this irrigation/rainfall event, the unstressed evapotranspiration rate and the average root depth and (iii) reducing the range of possible values for the hydraulic parameters to those that compute a time-to-stress that is consistent with the observed one, i.e. the difference between the observed water stress date and the date of the end of the last irrigation/rainfall event. The performance of this method is then checked for two sites within the frame of the SudMed and SALSA experiments by comparing the resulting properties to those obtained by other methods, namely the Beerkan infiltration test and the most commonly used pedotransfer functions. While not providing a unique set of hydraulic properties, the "evaporation test" is a good mean to refine the range of appropriate hydraulic parameter values at the scale of the Thermal Infra Red data.

Keywords : Soil hydraulic properties, pedotransfer functions, infiltration test, evaporation, water stress, TIR remote-sensing, SVAT model.

1. Introduction

Most water balance models, from the simplest ones (the FAO56 method, Allen et al., 1998) to the most complicated ones (complex SVAT schemes, hydrological models based on the Richards equation …) require an a priori knowledge of the soil hydraulic properties. Soil hydraulic properties can be classified in two types: textural properties, that describe the statistical distribution of the size of the pores, and structural properties, that describe the spatial organization and connectivity of the pores. Both property groups are linked since the biggest pore sizes induce the largest connectivity and therefore the highest conductivity. Texture maps are the most largely, and sometimes the only available information on soil properties at regional scale. Therefore, for most agronomical or hydrological applications, pedotransfer functions are applied to textural classes to derive soil hydraulic properties (Bouma, 1989). Pedotransfer functions are usually obtained from selected laboratory soil sample databases. Multivariate regression analyses are carried out to produce polynomial functions that link common retention and hydraulic conductivity curves (like the Brooks and Corey or the van Genuchten equations) to extended textural properties, at minimum clay and sand contents. Since these regressions are obtained from a limited number of samples, either stemming from a single region or from several laboratories (e.g. the Grizzly database, Haverkamp et al., 1997), their generality is rather questionable. Moreover, given the wide range of published pedotransfer functions (See Wagner et al., 2001, for a review) and the poor statistical link between structural and textural properties of a given soil, it is advisable to test the relevance of each of them before considering using one for a particular region/site of interest.

One possible way to check if one particular pedotransfer function can be applied locally is to perform lab analysis, but it is costly, both in time and money. A second approach is to carry out simple infiltration tests such as the Beerkan tests (Braud et al., 2005). Interpreting infiltration tests consists in matching cumulative infiltration curves for ponding (well permeameter, Beerkan and double-ring tests) or non-ponding (disc infiltrometer) conditions with simple analytical functions or more complex mathematical expressions such as the Richards equation (Zou et al., 2001; Ritter et al., 2004; Mynasni

et al., 2005) that depend on the local hydraulic properties. Since these tests rarely provide a single set of valid soil hydraulic parameters, alternative methods must be carried out to reduce the space of acceptable solutions. At the same (local) scale, evaporation tests have been carried out using vapour flux measurements (at the laboratory: Schneider et al., 2006). The physics of the extraction of vapour from the soil porous medium is strongly dependent on the movement of the liquid water below the evaporation front (Boulet et al., 1997) and, in turn, on the hydraulic properties. By minimizing the difference between the simulated and the observed vapour fluxes one can evaluate the hydraulic properties if an extra measurement of matric head and/or water content with time is available. Given the size of the ring or the evaporation chamber used in these methods, these tests provide point estimates of soil properties, whereas a global estimate at the scale of interest (usually the field) is required. There is therefore no direct means to access field-scale hydraulic data without a costly and time consuming lab or field study with multiple samples. Alternatively, eddy-correlation measurements of latent heat fluxes are usually based on a much larger footprint and can be considered as representative of the field; inverse methods consisting in minimizing the difference between the observed and the measured latent heat flux have been proposed, from synthetic (Jhorar et al., 2002) or observed (Gutmann and Small, 2007) evaporation data. But eddy-correlation systems are expensive and need well-trained staff to operate and maintain them. Furthermore, it is not possible to cover a large region in a short period except with a costly set-up.

Information on the water balance at the regional scale can be obtained routinely through the use of remote-sensing data. Several experiments have been carried out to test the assimilation of surface soil moisture inferred from active (Santanello et al., 2007) or passive (Burke et al., 1998) microwave remote-sensing data to constrain soil hydraulic properties. But soil moisture is not easy to observe through remote-sensing at an adequate resolution (for example the SMOS satellite mission will provide data on 0-5 cm soil moisture at ~50*50 km resolution) or with sufficient precision (radar data for instance is very sensitive to roughness and is usually acquired with a very sparse revisit period that is incompatible with most hydrological applications).

Amongst recent methods based on remote-sensing data, several papers have proposed to assimilate Thermal Infra Red (TIR) data into Soil Vegetation Atmosphere Transfer (SVAT) models (e.g. Demarty et al., 2004). In the near future, we expect that TIR remote-sensing data will be acquired every day or so at a resolution of less than 100m, which is consistent with the size of most agricultural

fields. Remote Sensing data in the TIR part of the spectrum provides indirect estimates of water stress – defined as a function of the ratio between actual and potential evaporation rates - at the earth surface. During the first stage of evaporation (“energy limited” evaporation) of an interstorm period, water availability is large enough to sustain evaporation at a potential rate and the ratio between actual and potential evapotranspiration is close to one: evapotranspiration depends only on the available energy at the surface. During the second stage of evaporation (“soil controlled” evaporation), the water content has dropped below a critical value and the diffusion processes within the soil are considerably reduced. This critical value depends on the hydraulic properties of the soil. Since the amount of soil water that can be easily extracted by roots is entirely controlled by the diffusion within the soil, transpiration decreases with diffusion, and stress occurs; as a result the ratio drops below one. During water stress, stomatal resistance is increasing and the available energy (mostly net radiation) is no longer converted into evaporation but in sensible heat. The latter is less efficient in dissipating energy and the surface of the leaves warms up. Surface temperature is thus strongly related to water stress. Since surface temperature can be deduced from TIR remote sensing data, stress and no-stress conditions can be observed from space. Data assimilation readjusts dynamically the soil water content and/or the soil parameters to minimize the difference between the simulated and the observed surface temperatures. Again, these methods are difficult to put into practice, and are meant to be applied over a long period of time. Indeed, potential differences in surface temperature are not always explained by inaccurate soil moisture content, but often as well by large errors in estimating the water and energy balance parameters. SVAT models have indeed a large number of unknown parameters, and the resulting observing system based on TIR data and SVAT models is usually underdetermined. Here, we propose a simpler procedure based on the same idea: can one relate water stress observed by TIR remote sensing for a given sensor resolution to the underlying soil physical properties at the same spatial resolution ? For that purpose, a simple yet robust evaporation equation (Boulet et al., 2000 and Boulet et al., 2004) for the second stage evaporation is used as a tool to check what soil parameter values are computing the same date for the onset of stress as what is observed under given conditions of uncertainty in the system. By restricting our study to water stress periods, i.e. periods for which second stage evaporation exists, and by using a simple but robust model, we ensure that the information extracted from TIR data is tightly linked to the diffusion processes within the soil and therefore to the prevailing soil hydraulic properties. The duration of the

first-stage drying, or time-to-stress, is so closely related to the hydraulic properties of the soil that it has been used as a surrogate to soil hydraulic properties by Salvucci (1997) for short vegetation. Levine and Salvucci (1999) have later on extended the approach to all vegetation types but this method requires time-to-stress observations for all interstorm periods, which gives little predictive value to the method. In order to get a comprehensive and predictive estimate of the whole water balance, one must have access to the soil hydraulic properties themselves. Contrarily to those approaches, that model evaporation by replacing the hydraulic properties with a function of an observed time-to-stress, Boulet et al. (2004) provide an analytical expression linking the time-to-stress to an average potential evapotranspiration rate, an average initial condition, and given soil hydraulic properties. Time-to-stress can thus be used to infer the latter if the two other inputs (potential evapotranspiration and initial soil moisture) are known. This paper builds on this hypothesis and presents an evaporation test designed to refine the range of acceptable soil hydraulic properties for use in a variety of water balance models. This test is based on the evaluation of the time-to-stress from TIR remote-sensing data and an analytical expression relating the time-to-stress to the hydraulic properties, the initial water content and a mean potential evaporation rate. The latter is derived from a simple energy balance equation driven by routinely available meteorological and ancillary remote-sensing data. In the second part of the paper, the performance of various methods to constrain soil hydraulic properties is analysed for data acquired during two international field experiments. These methods are (i) the proposed evaporation test, (ii) fitting the daily evaporation simulated by the SVATsimple model on the observed one, (iii) Beerkan infiltration tests and (iv) three commonly used pedotransfer functions.

2. Theoretical basis of the “evaporation test”

2.1. Concept

The principle of the evaporation test has been briefly outlined above and is relatively simple: the time-to-stress of a given surface is closely related to the amount of water that has been extracted at a potential rate from the beginning of the interstorm period (say, after a heavy rainfall or an irrigation

event); since this amount depends in turn on the hydraulic properties and the initial water content, it is possible to infer some information on those properties from an estimate of the time-to-stress if the latter is observable with TIR remote sensing data. The evaporation test consists in two successive modelling steps: First, a simple energy balance equation is solved to derive an average potential evapotranspiration rate and a related unstressed equilibrium surface temperature during each interstorm period for a given site. The difference between the unstressed and the observed surface temperature is then computed for all interstorm periods as a baseline to detect water stress (section 2.2). Second, a modelled time-to-stress (section 2.3) is calculated for all interstorm periods for which a reduction in evaporation due to water shortage is observed, using a range of realistic hydraulic parameter values. The parameter values that provide the smallest differences between the observed and the modelled time-to-stress are then kept as “appropriate”.

2.2. Detecting water stress using information in the Thermal Infra Red Spectrum

Water stress is classically related to a sharp increase in the difference between the surface temperature and the air temperature. However, it was shown in Boulet et al. (2007) that using solely the difference between the actual and a theoretical unstressed surface temperature is more efficient than using the classical index as a baseline to monitor water stress. To illustrate this, Figure 1 shows two dry-down periods selected for the B123 wheat field during the SudMed experiment (Chehbouni et al., 2008) in 2003, one when the field is a bare soil (top), the other at the end of the growing season of winter wheat (bottom). On the left hand side, evaporation time series in potential and real conditions are displayed; potential evaporation rates are simulated with a simple energy balance equation (Boulet et al., 2000), and the divergence between both evaporation curves corresponds to the time-to-stress. On the right hand side, time series of unstressed to observed surface temperature difference show a significant increase around the time-to-stress, while the difference between the surface temperature and the air temperature does not show a clear trend around that time.

In general, the simple energy balance model used to compute both the unstressed temperature T_{sp} and potential evaporation rate e_p is a simple “big-leaf” model with a single “bulk” source of energy. This description is consistent with the remote sensing data that do not discriminate between the different elements within a pixel. The interesting feature is that since the “evaporation

test" will be performed at the scale of the remote-sensing data, it provides an integrated or "effective" estimate of the hydraulic properties. An example of a simple "big leaf" model is provided in Boulet et al. (2007) and is given in Appendix. Following this approach, the data requirement to compute T_{sp} and e_p is then: (i) Meteorological forcing data and (ii) time series of Leaf Area Index (*LAI*), usually derived from time series of Normalised Differential Vegetation Index (NDVI) obtained from a combination of remotely sensed reflectances, and a given *LAI/NDVI* relationship (Duchemin et al., 2006).

2.3. An analytical expression of the "time-to-stress"

This section presents the analytical expression relating the time-to-stress to the amount of water that can be extracted by diffusion through the soil. For most models, the components of the water budget are obtained from a solution of the Richards (1931) equation under given initial and boundary conditions. During interstorm periods, those boundary conditions are made of an imposed flux (e_p) during the first stage of evaporation and an imposed (negative) pressure head during the second stage. Analytical simplifications of the Richards equation can be derived if the initial soil moisture profile is homogeneous. In that case, the transition from one stage to the other is solved by the Time Compression Approximation (Salvucci and Entekhabi, 1994). Let one use the following non-dimensional expressions of time t [T], readily available water in the root zone A [L] and evaporation rate e [LT^{-1}] (respectively):

$$\tilde{A} = 2A\left(\frac{K_0}{S_d^2}\right) \quad (1)$$

$$\tilde{t} = 2t\left(\frac{K_0}{S_d}\right)^2 \quad (2)$$

$$\tilde{e} = e / K_0 \quad (3)$$

A is the amount of water in the root zone that can be easily extracted by roots, i.e. the difference between the actual and the wilting point soil moisture multiplied by the effective root zone depth. This effective root zone depth corresponds to the soil volume that contains the largest percentage of the roots. K_0 [LT^{-1}] is the hydraulic conductivity and S_d [$LT^{-1/2}$] the desorptivity, both at initial water content. K_0 and S_d depend on (i) the initial water content θ_0 [-] at the beginning of the dry-down period, (ii) the

normalization parameters of the retention (saturated water content θ_{sat} [-] and air entry pressure h_g [L]) and conductivity (saturated hydraulic conductivity K_{sat} [LT^{-1}]) curves, that depend on the soil structure (Haverkamp et al., 1998) and are largely unknown and spatially variable and (iii) the shape factor of these two curves, that depend mostly on the soil textural properties and can be inferred from soil texture maps (Haverkamp et al., 2002).

In this study the van Genuchten retention curve (van Genuchten, 1980) relating water tension h [L] to soil volumetric moisture θ [-] under the Burdine assumption (Burdine, 1953) and the Brooks and Corey conductivity curve (Brooks and Corey, 1964) relating hydraulic conductivity K [LT^{-1}] to soil volumetric moisture θ were used:

$$\frac{K}{K_{sat}} = \left(\frac{\theta}{\theta_{sat}}\right)^{2+\frac{1}{m}} \text{ and } \frac{\theta}{\theta_{sat}} = \left[1+\left(\frac{h}{h_g}\right)^{\frac{2}{1-m}}\right]^{-m} \tag{4}$$

Where m [-] is a shape factor. In that case (see Boulet et al., 2004 for details):

$$S_d^2 = \frac{4K_{sat}h_g(1-m)}{3}c_p(\theta_0,\theta_{sat},m) \text{ and } \frac{K_0}{K_{sat}} = \left(\frac{\theta_0}{\theta_{sat}}\right)^{2+\frac{1}{m}} \tag{5}$$

$$c_p(\theta_0,\theta_{sat},m) = \theta_0 \mathrm{B}_{x,a,b}\left(\left(\frac{\theta_0}{\theta_{sat}}\right)^{\frac{1}{m}}, \frac{5m+1}{2}, \frac{1-m}{2}\right) - \theta_{sat}\mathrm{B}_{x,a,b}\left(\left(\frac{\theta_0}{\theta_{sat}}\right)^{\frac{1}{m}}, \frac{7m+1}{2}, \frac{1-m}{2}\right) \tag{6}$$

where

$$\mathrm{B}_{x,a,b}(x,a,b) = \int_0^x u^{a-1}(1-u)^{b-1}du \tag{7}$$

is the product of the Incomplete Beta function $I_x(a,b)$ and its corresponding Beta function $B(a,b)$ (*Press et al.,* 1992, p. 219).

It has been shown (see Boulet et al., 2004 for details) that the instantaneous evaporation can then be expressed as:

$$\begin{cases} \forall \tilde{t} \le \tilde{t}_{stress}, \tilde{e}(\tilde{t}) = \tilde{e}_p \\ \forall \tilde{t} > \tilde{t}_{stress}, \dfrac{1}{\tilde{e}(\tilde{t})} = \tilde{t} - \tilde{t}_{stress} + \tilde{A} - \tilde{t}_{stress}\tilde{e}_p + \dfrac{\tilde{t}_{stress}}{\tilde{t}_{stress}\tilde{e}_p - \tilde{A}} + \ln\left(1+\dfrac{1}{\tilde{e}(\tilde{t})}\right) \end{cases} \tag{8}$$

where the nondimensional time-to-stress $\tilde{t}_{stress}$ is the solution of:

$$e^{\tilde{t}_{stress}\tilde{e}_p-\tilde{A}} = 1+\frac{\tilde{t}_{stress}}{\tilde{t}_{stress}\tilde{e}_p-\tilde{A}} \quad (9)$$

It follows from Equation 2:

$$t_{stress}=\frac{1}{2}\left(\frac{S_d}{K_0}\right)^2\tilde{t}_{stress} \quad (10)$$

Equations 1-10 are used together with the simple energy balance described in Appendix to build the simple yet physically-based single source/single bucket SVATsimple model.

Time-to-stress t_{stress} is thus derived from Equations 9 and 10 from an estimate of e_p, hydraulic properties, root depth and average initial water content. Again, only the shape factor of the retention and conductivity curves (m) is related dominantly to soil texture, while the three normalization parameters (θ_{sat} and, to a larger extent, K_{sat}, and h_g) depend mainly on soil structure. It is therefore difficult to estimate them from textural properties alone, as it is done traditionally with the pedotransfer functions. Consequently, the evaporation test consists in minimizing the difference between the observed and the simulated time-to-stress by adjusting the two main normalization parameters, K_{sat} and h_g.

3. Application and comparison with Beerkan tests and Pedotransfer functions

3.1. Field data

Two interstorm periods have been selected for both the B123 (Figure 1) and the SALSA (Semi Arid Land Surface Atmosphere, Goodrich et al., 2000) experiments (see Boulet et al., 2007 for details on both datasets). For B123, soil moisture limits the evaporation of the wheat field at two classical stages in the agricultural calendar: one after the first irrigation following sowing, and one after the last irrigation when wheat is mature. For the SALSA experiment, the vegetation is a sparse grassland, and both water stress events are located at the end of the growing period during the summer monsoon, with slightly wetter conditions for the first interstorm. B123 is a clay loam (clay fraction is 35% clay and

sand fraction is 23%), while SALSA Zapata site is a sandy loam (clay fraction is 8% and sand fraction is 67%). Saturated water content is derived from bulk density measurements as a fixed proportion (90%) of the porosity, following Rogowski (1971).

In both cases, time series of actual evapotranspiration measured by eddycorrelation systems are available but no hydraulic property has been measured in the laboratory, except for one disturbed sample taken at the surface (a few cm) of the B123 site, for which PF 4.2, PF 3, PF 2.5 and PF 2 soil moisture values have been measured. In both experiments, surface temperature is observed by in-situ thermoradiometers. The measurement footprint ranges from a few square meters for the radiometers to a few hectares for the eddy-correlation system that estimates the latent heat flux. As mentioned before, evapotranspiration is difficult to measure and needs a well-trained staff to operate the system whereas an in-situ thermoradiometer is easy to install. Moreover, even though current satellite platforms cannot provide any data at a satisfactory spatial (<100m) and temporal (1 acquisition per day) resolutions, one hopes that high resolution TIR images will be routinely acquired in the near future. In that case the proposed evaporation test could be applied more operationally. It is thus important to keep in mind that even though a performance criterion using the evaporation data will be developed in the next section to evaluate the method, the proposed methodology (the “evaporation test”) relies on the minimization between the "observed" and simulated time-to-stress inferred from remote-sensing.

Hydraulic properties for the B123 site have been estimated through infiltration tests. Those tests provide an independent evaluation of the performance of the “evaporation test”. Infiltration tests are based on fitting an analytical approximation of the Richards (1931) equation to an observed infiltration rate. The approximation is usually obtained for homogeneous initial conditions and under constant positive head and assumes that a pseudo-constant water depth is applied at the soil surface. Here we implemented the Beerkan method (Braud et al., 2005), which fits this analytical approximation on an experimentally derived cumulative infiltration curve. The latter is obtained by pouring a given amount of water in a ring sitting on the soil surface, waiting for it to disappear in the ground, noting the corresponding time with a stopwatch and repeating this operation until the steady-state flow is reached. 115 Beerkan tests have been carried out in the Haouz plain over selected fields in the irrigation district where the B123 site is located. Amongst those 115 tests, 12 Beerkan tests have been performed in the B123 field itself. The resulting h_g and K_{sat} values for the 115 tests and the

whole range of textural properties present in the irrigation district are shown on Figure 2, alongside with those derived from the widely used pedotransfer function of Clapp and Hornberger (1978). All solutions of the Beerkan tests for each textural class are kept and shown on Figure 2 as a mean value and an error bar. Despite the decrasing trend in both hydraulic parameter values across the range of clay percentages, as documented by the parabolic regression, the large error bars and the large scatter of points show the large variability of parameter values within each textural class. This variability cannot be represented by the pedotransfer function and we describe below how both infiltration and evaporation tests can complete this information.

3.2. Diagnostic variables and inversion methods

3.2.1. Improving model parameterization during no stress periods

One expects that the usefulness of the “evaporation test” will largely depend on the accuracy of the numerous input data, including the potential evapotranspiration rate e_p. Given the uncertainty on e_p estimates derived from any “big leaf” model, it is advisable to use TIR data also to reduce the bias between the observed and the simulated latent heat flux in potential conditions, i.e. before the onset of stress. Indeed, even if with current satellite retrieval capabilities one can expect in the near future an overall measurement error of the order of 1°K, this error is generally small compared to the typical model error one obtains when the most sensitive parameters of the energy balance model are not known a priori. Comparing the observed and the computed surface temperature during no stress periods can help optimize the model parameterization. By choosing a-priori ranges of values for the most sensitive parameters (see Table 1), namely the minimum surface resistance, the soil heat flux to net radiation ratio under bare soil conditions and the parameter governing the difference between the aerodynamic and the surface temperature, an ensemble of potential evapotranspiration values can be generated with the simple “big leaf” model. From this ensemble one can compute a standard deviation of e_p. which will be used as an error estimate in the uncertainty framework presented below for the second step of the evaporation test. For the second (full cover conditions) stress period of the B123 site, the temperature simulated by the simple energy balance using the middle of the ranges of values given in Table 1 is already close to the observed surface temperature (Figure 1). By selecting the parameter values that produce an average absolute bias between the simulated and the observed

surface temperature before the time-to-stress that is lower than 1°C, the standard deviation of the latent heat flux is considerably reduced: It drops from 0.46 mm/day to 0.27 mm/day (Figure 3). It is noticeable that the difference between the observed and the simulated evapotranspiration during this no stress period is also reduced (from 0.13 mm/day to 0.07 mm/day). For bare soil conditions, observations are very far from the range of simulated temperature values (Figure 1) and this distance cannot be reduced by fitting the parameters within the ranges given in Table 1. The average standard deviation is not reduced by TIR data assimilation and the expected error without TIR data assimilation (also of the order of 0.27 mm/day) is kept in the second step of the evaporation test.

3.2.2. Diagnostic variables of the model performance for evaporation and time-to-stress

In order to evaluate the amount of information contained in the sole time-to-stress observation compared to a complete evaporation time series, two separate criteria will be computed to select the appropriate hydraulic properties $[h_g, K_{sat}]$. The first criterion is only used to evaluate the method. It is based on the mean distance between the simulated (Eq. 8) instantaneous evaporation and the observed evaporation time series. A Nash efficiency is computed for all possible combinations of realistic hydraulic property values. We identify the overall maximum efficiency, and then select arbitrarily all solutions that lead to a Nash efficiency greater than 90% of the overall maximum as "acceptable". Nash efficiency E is given as:

$$E = 1 - \frac{\overline{e_{sim}^2 - e_{obs}^2}}{\overline{e_{obs}^2 - \overline{e_{obs}^2}}} \quad (10)$$

Where e_{sim} and e_{obs} are the simulated and observed daily evaporation rates, and $\bar{}$ stands for "average value over the calibration window", respectively.

The second criterion is meant to be used routinely in the "evaporation test". It is based on the difference between the observed (Eq. 10) and the simulated time-to-stress. Since the observed time-to-stress is likely to be derived from trend analysis with daily TIR observations, its precision is larger than a day. We therefore select all possible hydraulic property values that lead to a difference between the observed and the simulated time-to-stress of less than 1 day.

In order to produce maps of the two criteria (Nash efficiency for evaporation and difference in time-to-stress) in the $[h_g, K_{sat}]$ parameter space, simulations were carried out for both interstorm periods of each site. The uncertainty framework takes into account errors in initial water content, potential

evapotranspiration (as obtained from section 3.2.1), and shape factors of the retention and conductivity curves. K_{sat} and h_g values are chosen from within the realistic predefined ranges given in Table 1. Initial water content and root zone depth are evaluated locally at three locations within each field from gravimetric and bulk density measurements and an allometric survey (respectively). The root zone depth is different from the maximum root extent but coincides with the zone of maximum root density (around 20 cm in the case of the wheat). It can increase as *LAI* increases but in our case it is kept constant since all dry-down periods are located either at the end of the growing season or when vegetation is absent (A=0). Due to the difficulty to evaluate the extent of the root zone depth, it is important to use the same value for the evaporation test and the model for which an estimate of the hydraulic parameters is required. The shape factors of the retention and conductivity curves are deduced from the particle size distribution with Fractal Similarity following the method given by Braud et al. (2005). The search algorithm scans systematically the possible range of values by incrementing each parameter from the minimum to the maximum defined in Table 1 and investigating all combinations of the seven following quantities: h_g, K_{sat}, the shape factor of the Van Genuchten retention curve, the initial water content and the mean potential evaporation rate before the the onset of stress for both drydowns. Figure 4 shows a superposition of the contour plots for both criteria in the $[h_g, K_{sat}]$ parameter space. Each criterion is made of a composite of the two criteria values for the two dry-downs, weighted by the number of days in each dry-down. In order to produce this contour plot in a 7D optimization problem, only the optimal values of each criterion with respect to the five remaining parameters are shown in this Figure. The optimal set of the last five parameters for each $[h_g, K_{sat}]$ value corresponds to the highest Nash for the evaporation criterion and the lowest difference in time for the “evaporation test” criterion.

3.2.3. Diagnostic variables for the Beerkan tests

Because of the limited time available to perform each infiltration test, the number of points on each cumulative infiltration curve is rather small (4 to 9 volumes of 200 ml). Consequently, special care must be taken to select the appropriate *[hg, Ksat]* solutions when interpreting the tests. Two criteria were chosen for assessing the accuracy of the retrieved parameters:

(i) The number of solutions in the predefined parameter-space (same range as in Table 1) and (ii) the Root-Mean-Square-Error (RMSE) between the simulated and the observed cumulative infiltration

curves. These two criteria are used for evaluation only, not the selection of the appropriate hydraulic parameters. Therefore, all solutions are shown in what follows and the criteria allow assigning a quality tag to each test.

3.3. Results

For B123, the best-fit $[h_g, K_{sat}]$ values are organized along a crest of Nash efficiency in the $[h_g, K_{sat}]$ parameter space, making impossible to select one particular solution. This is consistent with findings by Zou et al. (2001) on soil properties retrieval from soil moisture observations. It is also consistent with the expression of the desorptivity (Equation 5) since the amount of water that can be extracted by diffusion is proportional to both h_g and K_{sat}. Due to the expected errors in field average initial water content and potential evapotranspiration, the segment of "acceptable" h_g and K_{sat} values occupies a much larger proportion of the parameter space than if those quantities were known with absolute precision.

The space defined by the contour lines with a time-to-stress difference of less than one day is consistent with the space between the contour lines of positive Nash efficiency values. Time-to-stress difference increases sharply from less than a day to values much larger than 5 days. Figure 5 shows the pattern of $[h_g, K_{sat}]$ values selected as "acceptable solutions" according to both criteria and following the increment used in the search algorithm. It also shows the solutions of the Beerkan infiltration tests (crosses) and the values given by the traditionally used Clapp and Hornberger (1978) pedotransfer function (stars). These solutions will be intercompared in the next section. As expected, the number of possible parameter values is much more limited with the first (efficiency, open squares) rather than with the second (time difference, filled dots) criterion: the evaporation time-series, including the amplitude and time-scale of the evaporation reduction after the onset of stress, contain more information on the second stage of evaporation than the sole time-to-stress.

For the SALSA data set (Figures 6 and 7), there is again a much smaller zone with acceptable solutions for the first criterion (Nash efficiency) than for the second one (difference in time to stress). Indeed, for all h_g and K_{sat} values above a certain threshold (around -0.1 m and 10^{-5} m/s respectively), the large water loss by gravitational drainage implies that stress occurs in the early days of the drying cycle. In that case, the decline in daily evaporation over time during the second stage contains a large

amount of information on the moisture diffusion processes within the soil, compared to the sole time-to-stress, and the first criterion enables to reduce at least the space of acceptable air entry pressure values to the [-0.2,-2] range. On the other hand, even if stress occurs on the very first day, as is the case for the second SALSA drying down period, the time-to-stress and the Nash efficiency on evaporation lead one to accept all K_{sat} values above 10^{-5} m/s, which means that the abrupt decrease in evaporation during Stage Two does not result in extra information compared to the time-to-stress.

3.4. Comparison with Beerkan tests and pedotransfer functions

Results for the 12 tests performed at the B123 site are shown as plusses on Figure 5; all solutions of the tests are shown, but, following the criteria presented above, the best Beerkan results are obtained for the isolated groups of plusses which mostly correspond to the lowest RMSE, while for the lowest *hg* and K_{sat} values the fit is poor and there are many solutions along a straight line in the $[h_g, K_{sat}]$ log-log space. Again, this is consistent with the expression of the sorptivity (see Braud et al., 2005) since the amount of water that can infiltrate by diffusion, a dominant process for low h_g and K_{sat} values, is proportional to both h_g and K_{sat}. The solutions of the Beerkan tests are also organized along a power-shape curve in the $[h_g, K_{sat}]$ log-log space. This curve crosses the line of the solutions given by the evaporation test for medium $[h_g, K_{sat}]$ values corresponding to the Clapp and Hornberger (1978) estimates for a clay loam and a silty clay loam (stars). One must note that also the hydraulic parameters always correlate to some extend it is notable that here *hg* and K_{sat} were derived for the Clapp and Hornberger models that are different from the van Genuchten and Burdine models. Altogether, there is a good agreement between the three estimates since all solutions intersect at approximately K_{sat} = 2 10^{-6} m/s and h_g = -0.4 m . This means that if one single method does not provide a narrow range of values, estimates can be combined to significantly reduce the overall range of parameters by keeping all values that show consistency with all three methods. One can assume that the alignment of all solutions along a curve either concave-up or concave-down in the $[h_g, K_{sat}]$ space is linked to the mathematical form of either the evaporation or the infiltration curve. Finally, all estimates of the resulting wilting point and field capacity are compared (Table 2) with additional pedotransfer functions proposed by Rawls and Brakensiek (1985) and Saxton and Rawls (2006) which are based on other mathematical expressions of the retention curve than the van Genuchten equation.

The mean, minimum and maximum values given by each method are very different, but there is always a substantial overlap between all estimates. Note that the single retention curve measured in the laboratory from an undisturbed sample taken from the first 10 cm of the soil surface provides values in the lower part of all ranges of values, with a field capacity of 0.35 m^3/m^3 and a wilting point of 0.20 m^3/m^3. By fitting the Van Genuchten model to this experimental retention curve, a value of h_g of -0.41 m is obtained, which is consistent with the intersection of all estimation methods. However, the retrieved *m* value (0.07) is larger than the one obtained by Fractal Similarity (0.05).

For the SALSA dataset, the Clapp and Hornberger (1978) pedotransfer function [h_g, K_{sat}] values for sandy loam (star in Figure 6) are within the range of acceptable solutions given by the evaporation test (filled dots), but the air entry pressure is less negative than that provided by the evaporation criterion (open squares).

4. Conclusion

The principles of an "evaporation test" using remotely sensed TIR data have been presented in this paper. The "evaporation test" consists of two parts:

(i) detecting water stress as a sharp divergence between the observed and the unstressed surface temperature time series and inverting the unknown parameters of the energy budget by minimizing the difference between both temperatures before the onset of stress (information used : TIR and Normalized Differential Vegetation Index NDVI data at representative scale; NDVI/Leaf Area Index relationship; meteorological data) and

(ii) selecting the hydraulic parameters *[h_g, K_{sat}]* that give a simulated time-to-stress consistent with the observed time-to-stress (information used: difference between the date of last irrigation or rainfall and the time-to-stress derived in the previous step; water content at the beginning of the interstorm period; particle size distribution; estimate of the root zone depth).

This method allows for refining the range of valid hydraulic properties at the scale of the remote-sensing measurements. The obtained range of values has been compared to i) the amount of information one can retrieve from observed evaporation time series and ii) local estimates of the hydraulic properties deduced from infiltration tests. It has been shown that deriving a rough estimate of the time-to-stress from remote-sensing yields significant information on the appropriate hydraulic properties compared to the evaporation time series measured by an eddy-correlation device.

Moreover, the soil hydraulic properties inferred from this estimate, although spanning a wide range of values in the hydraulic conductivity / retention curve parameter space, are consistent with the estimates obtained by other means (pedotransfer functions and infiltration tests). The main advantage of this method is that the information retrieved from TIR data is representative of the pixel size of the TIR imagery. The main limitation of this method is that a field average initial soil moisture is difficult to assess, especially with remote-sensing; a possible way to bypass this for irrigated agriculture is to assume that initial water content is close to field capacity, but this remains a very crude estimate. Moreover, if several land uses or irrigation practices are present in the pixel, the results of the method are representative of an average water stress, even if such a stress occurs only on part of the pixel. Further work should therefore address the scaling relationship between the evaporation time series simulated using these average parameters and the sum of the weighted individual flux estimates for each homogeneous unit of an heterogeneous pixel. Finally, it is expected that this method will be more easily implemented in arid and semi-arid climates rather than in temperate regions where dry periods are not very long and where water stress is seldom reached.

Acknowledgments

This study was conducted within the framework of the IRD/Sud-Med project, with support from the European Union 5th Framework through the INCO-MED Program IRRIMED (http://www.irrimed.org/) and the integrated action French-Morocco PAI n°MA/06/148. Additional funding was provided through EU Pleiades project as well as CNES/TOSCA program. The authors would like to acknowledge the Sud-Med technical partners, and especially ORMVAH (Office Regional de Mise en Valeur Agricole du Haouz). All reviewers are thanked for their constructive comments that greatly improved the paper.

Appendix: the Simple "big leaf" energy balance model (Boulet et al., 2000)

T_{sp} is the solution of the following energy balance equation:

$$\left[(1-a_s)Rs + \sigma\varepsilon_s\left(\varepsilon_a T_a^{\,4} - T_{sp}^{\,4}\right)\right](1-\xi(L)) = \rho c_p \zeta\left(\frac{T_{sp}-T_a}{r_a(T_{sp})}\right) + \frac{\rho c_p}{\gamma}\left(\frac{e^*\left[T_0(T_{sp})\right]-e_a}{r_a(T_{sp})+r_s(L)}\right)$$

where ρ is the air density, c_p is the specific heat of air at constant pressure, a_s is the surface albedo, *Rs* the incoming solar radiation, ε_s the surface emissivity, ε_a the air emissivity, σ the Stefan-Boltzman constant, T_a the air temperature, soil heat flux *G* is a fraction $\xi(L) = \xi_s e^{-0.4L}$ of the net radiation *Rn* depending on the Leaf Area Index (*L*) and an empirical parameter ξ_s, T_{0p} is the aerodynamic temperature, $\zeta = \frac{T_{0p} - T_a}{T_{sp} - T_a} = 1 - \frac{e^{-[\ln(L)-\mu]^2/1.6}}{0.8L\sqrt{2\pi}}$ relates T_{0p} to the surface temperature T_{sp} according to *L* and an empirical parameter μ, $r_a = r_{a0} \frac{1}{(1 + \mathrm{Ri}(T_0(T_{sp}) - T_a))^{\eta}}$ is the aerodynamic resistance relating the aerodynamic resistance without stability correction r_{a0} to the Richardson number Ri which is a function of the T_{sp}-T_a difference, η = 0.75 in unstable conditions and $\eta = 2$ in stable conditions, e^* is the saturation vapour pressure at a given temperature, e_a is the current air vapour pressure, $r_s(L) = \begin{cases} r_{c\min} L & \text{if} \quad L < 1 \\ r_{c\min}/L & \text{if} \quad L \geq 1 \end{cases}$ is the surface resistance and r_{cmin} the minimum stomatal resistance.

One can note that with the above notations $\lambda e_p = \frac{\rho c_p}{\gamma} \left(\frac{e^*(T_0(T_{sp})) - e_a}{r_a(T_{sp}) + r_s(L)} \right)$

References

Allen, R.G., Pereira, L.S., Raes, D., Smith, M., Crop evapotranspiration: guidelines for computing crop water requirements, *FAO Irrigation and Drainage Paper* **56**, Rome, (1998), 300 pp.

Boulet G., Chehbouni A., Gentine P., Duchemin B., Ezzahar J., Hadria R., Monitoring water stress using time series of observed to unstressed surface temperature difference, *Agricultural and Forest Meteorology*, **146** (2007), pp. 159-172.

Boulet G., A. Chehbouni, I. Braud, B. Duchemin and A. Lakhal, Evaluation of a two-stage evaporation approximation for contrasting vegetation cover, *Water Resources Research*, **40** (2004), W12507, doi:10.1029/2004WR003212.

Boulet, G., Chehbouni, A., Braud, I., Vauclin, M., Haverkamp, R. and Zammit, C., A simple water and energy balance model designed for spatialisation and remote sensing data utilization, *Agricultural and Forest Meteorology*, **105** (2000), pp. 117-132.

Boulet, G., Braud. I. and Vauclin, M., Study of the mechanisms of evaporation under arid conditions using a detailed model of the soil-atmosphere continuum. Application to the EFEDA I experiment, *Journal of Hydrology*, **193** (1997), pp. 114-141.

Bouma, J., Using soil survey data for quantitative land evaluation, *Advances in Soil Science*, **9** (1989), pp. 177–213.

Braud, I., D. De Condappa, J. M. Soria, R. Haverkamp, R. Angulo-Jaramillo, S. Galle, M. Vauclin, Use of scaled forms of the infiltration equation for the estimation of unsaturated soil hydraulic properties (the Beerkan method), *European Journal of Soil Science*, **56**(3) (2005) pp. 361–374.

Brooks, R.H. and Corey, A.T., Hydraulic properties of porous media, *Hydrology paper*, **3** (1964) Colorado State University, Fort Collins.

Burdine, N.T., Relative permeability calculation from size distribution data, *Transactions AIME*, **198** (1953), pp. 71-78.

Burke, E. J., Gurney, R. J., Simmonds, L. P., and O'Neill, P. E., Using a modeling approach to predict soil hydraulic properties from passive microwave measurements, *IEEE Transactions on Geoscience and Remote Sensing*, **36** (1998), pp. 454−462.

Chehbouni, A., Escadafal, R., Duchemin, B., Boulet, G., Simonneaux, V., Dedieu, G., Mougenot, B., Khabba, S., Kharrou, H., Maisongrande, P., Merlin, O., Chaponniere, A., Ezzahar, J., Er-Raki, S., Hoedjes, J., Hadria, R., Abourida, A., Cheggour, A., Raibi, F., Boudhar, A., Benhadj, I., Hanich, L., Benkaddour, A., Guemouria, N., Chehbouni, A.H., Lahrouni, A., Olioso, A., Jacob, F., Williams, D.G. and Sobrino, J.A. An integrated modelling and remote sensing approach for hydrological study in arid and semi-arid regions: the SUDMED programme, *International Journal of Remote Sensing*, **29**(17-18)(2008), pp. 5161-5181.

Clapp R.B. and G.M. Hornberger, Empirical equations for some soil hydraulic properties, *Water Resources Research*, **14**(4) (1978) pp. 601-604.

Demarty, J., C. Ottlé, I. Braud, A. Olioso, J.P. Frangi, L. Bastidas, H.V. Gupta, Using a multiobjective approach to retrieve information on surface properties used in a SVAT model, *Journal of Hydrology*, **287** (2004), pp. 214-236.

Duchemin B., Hadria R., Er-Raki S., Boulet G., Maisongrande P., Chehbouni A., Escadafal R., Ezzahar J., Hoedjes J., Kharrou M.H., Khabba S., Mougenot B., Olioso A., Rodriguez J-C., Simonneaux V., Monitoring wheat phenology and irrigation in Center of Morocco: on the use of relationship between evapotranspiration, crops coefficients, leaf area index and remotely-sensed vegetation indices, *Agricultural Water Management*, **79** (2006), pp. 1-27.

Goodrich, D.C., Chehbouni, A., Goff, B., MacNish, B., Maddock, T., Moran, S., Shuttleworth, W. J., Williams, D. G., Watts, C., Hipps, L. H., Cooper, D. I., Schieldge, J., Kerr, Y. H., Arias, H., Kirkland, M., Carlos, R., Cayrol, P., Kepner, W., Jones, B., Avissar, R., Begue, A., Bonnefond, J. -M., Boulet, G., Branan, B., Brunel, J. P., Chen, L. C., Clarke, T., Davis, M. R., DeBruin, H., Dedieu, G., Elguero, E., Eichinger, W. E., Everitt, J., Garatuza-Payan, J., Gempko, V. L., Gupta, H., Harlow, C., Hartogensis, O., Helfert, M., Holifield, C., Hymer, D., Kahle, A., Keefer, T., Krishnamoorthy, S., Lhomme, J.-P., Lagouarde, J.-P., Lo Seen, D., Luquet, D., Marsett, R., Monteny, B., Ni, W., Nouvellon, Y., Pinker, R., Peters, C., Pool, D., Qi, J., Rambal, S., Rodriguez, J., Santiago, F., Sano, E., Schaeffer, S. M., Schulte, M., Scott, R., Shao, X., Snyder, K. A., Sorooshian, S., Unkrich, C. L., Whitaker M., Yucel, I., Preface paper to the Semi-Arid Land-Surface-Atmosphere (SALSA) Program special issue, *Agricultural and Forest Meteorology*, **105**(1-3) (2000), pp. 3-20.

Gutmann, E. D. and E. E. Small, A comparison of land surface model soil hydraulic properties estimated by inverse modeling and pedotransfer functions, *Water Resources Research,* **43**(5) (2007), W05418, doi:10.1029/2006WR005135.

Haverkamp, R., Zammit, C., Bouraoui, F., Rajkai, K., Arrúe, J. L. and N. Heckmann, GRIZZLY, Grenoble Soil Catalogue: Soil survey of field data and description of particle size, soil water retention and hydraulic conductivity functions. Laboratoire d'Etude des Transferts en Hydrologie et Environnement (LTHE), Grenoble Cedex 9, France, (1997).

Haverkamp, R., Bouraoui, F., Angulo-Jaramillo, R., Zammit, C. and J.W. Delleur, Soil properties and moisture movement in the unsaturated zone. In: CRC Groundwater Engineering Handbook (ed. J.W. Delleur), pp. 5.1–5.50. CRC Press, Boca Raton, FL, (1998).

Haverkamp, R., Nimmo, J.R. and P. Reggiani, Property-transfer models. In: Methods of Soil Analysis: Part 4, Physical Methods (eds J.H. Dane & C.G. Topp), pp. 759–782. Monograph No 5, Soil Science Society of America, Madison, WI (2002).

Jhorar, R.K., Bastiaanssen, W.G.M., Feddes, R.A. and J.C. Van Dam, Inversely estimating hydraulic functions using evapotranspiration fluxes, *Journal of Hydrology*, **258** (2002) pp. 198-231.

Levine, J. B. and Salvucci, G.D., Characteristic rate scale and timescale of supply-limited transpiration under a Richards-Cowan framework. *Water Resources Research,* **35**(12) (1999) pp. 3947-3954.

Minasny B. and Field D.J., Estimating soil hydraulic properties and their uncertainty: the use of stochastic simulation in the inverse modelling of the evaporation method, *Geoderma*, **126**(3-4) (2005), pp. 277-290.

Press, W.H., Teukolski, S.A., Vetterling, W.T. and B.P. Flannery, Numerical Recipes in FORTRAN Second Edition, Cambridge University Press, Cambridge, UK, 964 pp,(1992).

Richards, L. A., Capillary conduction of liquids through porous media, *Physics,* **1** (1931) pp. 318-333.

Rawls, W.J., Brakensiek, D.L., 1985. Prediction of soil water properties for hydrologic modelling. In: Jones, E., Ward, T.J. (Eds.). Watershed Manag. Eighties. Proceedings of Symposium ASCE, Denver, CO, 30 April-2 May 1985, ASCE, New York, pp. 293-299.

Ritter, A., R. Muñoz-Carpena, C. M. Regalado, M. Vanclooster and S. Lambot. Analysis of alternative measurement strategies for the inverse optimization of the hydraulic properties of a volcanic soil. *Journal of Hydrology*, **295**(1-4) (2004), pp. 124-139.

Rogowski, A.S., Watershed physics: Model of soil moisture characteristics, *Water Resources Research*, **7**(6) (1971) pp. 1575-1582.

Salvucci, G. D., Soil and moisture independent estimation of stage-two evaporation from potential evaporation and albedo or surface temperature, *Water Resources Research*, **30**(1) (1997) pp. 111-122.

Salvucci, G. D., and D. Entekhabi, Equivalent steady soil moisture profile and the time compression approximation in water balance modeling, *Water Resources Research*, **30** (1994) pp. 2737-2749.

Santanello Jr, J.A., Peters-Lidard, C.D., Garcia, M.E., Mocko, D.M., Tischler, M.A., Moran, M.S. and Thoma, D.P., Using remotely-sensed estimates of soil moisture to infer soil texture and hydraulic

properties across a semi-arid watershed. *Remote Sensing of Environment*, **110**(1) (2007), pp. 79-97.

Saxton, K. E. and W. J. Rawls, Soil water characteristic estimates by texture and organic matter for hydrologic solutions, *Soil Science Society America Journal*, **70** (2006) pp. 1569–1578.

Schneider, K., Ippish, O., K. Roth, Novel evaporation experiment to determine soil hydraulic properties, *Hydrology and Earth System Sciences*, **10** (2006) pp. 817-827.

Van Genuchten, M.T., A closed-form equation for predicting the hydraulic conductivity of unsaturated soils, *Soil Science Society America Journal*, **44** (1980) pp. 892-898.

Wagner, B., Tarnawski, V.R., Hennings, V., Müller, U, Wessolek, G. and R. Plagge, Evaluation of pedo-transfer functions for unsaturated soil hydraulic conductivity using an independent data set, *Geoderma*, **102** (2001) pp. 275-297.

Zou, Z.-Y., M.H. Young, Z. Li and P.J. Wieranga, Estimation of depth averaged unsaturated soil hydraulic properties from infiltration experiments, *Journal of Hydrology*, **242** (2001), pp. 26-42.

Figure and Table captions

Figure 1. Evaporation and temperature time series for two dry-down periods of the 2003 B123 wheat growing season: bare soil (top) and full cover (bottom); the vertical bar indicates the onset of stress.

Figure 2. Saturated hydraulic conductivity and air entry pressure values obtained for the 115 Beerkan tests in the Haouz plain, along with the interpolated Clapp and Hornberger (1978) pedotransfer function, plotted against clay fraction.

Figure 3. Daily evaporation time series for the second dry-down period of the 2003 B123 wheat growing season: simulation results before (a) and after (b) the minimization on the observed surface temperature time series in potential conditions.

Figure 4. Nash efficiency between the observed and the simulated daily evaporation time series (contour filled) and difference between the observed and the simulated time-to-stress (contour lines) in the saturated hydraulic conductivity K_{sat}/air entry pressure h_g parameter space for the B123 site.

Figure 5. Selected saturated hydraulic conductivity K_{sat}/air entry pressure h_g parameter values deemed "acceptable" for the B123 site: according the Nash criteria for evaporation (empty squares) and the difference in time-to-stress (filled dots); stars show the value given by the Clapp and Hornberger (1978) pedotransfer function for a clay loam and a silty clay loam; crosses show the results of the 12 Beerkan tests performed in the B123 field.

Figure 6. same as Figure 4. for the SALSA grassland site (Zapata).

Figure 7. same as Figure 5. for the SALSA grassland site (Zapata); the star shows the value given by the Clapp and Hornberger (1978) pedotransfer function for a sandy loam.

Table 1. Parameter range used in this study.

Table 2. Field capacity and wilting point values obtained with different methods for the B123 site.

Table 1

parameter	range
Saturated hydraulic conductivity K_{sat} [m/s]	$1x10^{-7}$.. $5x10^{-5}$
Air entry pressure h_g [m]	-12.. –0.03
Shape factor of the retention curve m [-]	0.04..0.05 (B123) and 0.06..0.07 (Zapata)
Initial water content θ_0 [-]	observed initial water content +/-0.03
Minimum surface resistance r_{cmin} [s/m] [1]	50..150
Albedo a_s [-][1]	0.11..0.15 (soil) and 0.15..0.2 (vegetation)
Soil heat flux to net radiation fraction ξ_S [-][1]	0.2..0.5 (bare soil conditions)
Parameter μ [-][1]	0.1..1
Root zone depth [m][2]	0.2

[1] See Appendix for the explanation of the symbol;

[2] Root zone depth was fixed *a priori* in order to downsize the number of acceptable solutions;

1 Table 2

2

		Beerkan tests	Evaporation tests	Clapp and Hornberger (1978)	Rawls and Brakensiek (1985)	Saxton and Rawls (2006)	GRIZZLY database	Surface soil sample (laboratory)
Field capacity [m^3/m^3]	Min	0.25	0.31	0.36	0.25			
	Mean	0.36			0.34	0.35	0.38	0.35
	Max	0.40	0.41	0.39	0.42			
Wilting point [m^3/m^3]	Min	0.17	0.22	0.22	0.14			
	Mean	0.25			0.22	0.20	0.25	0.20
	Max	0.33	0.35	0.25	0.31			

3

Figure 1

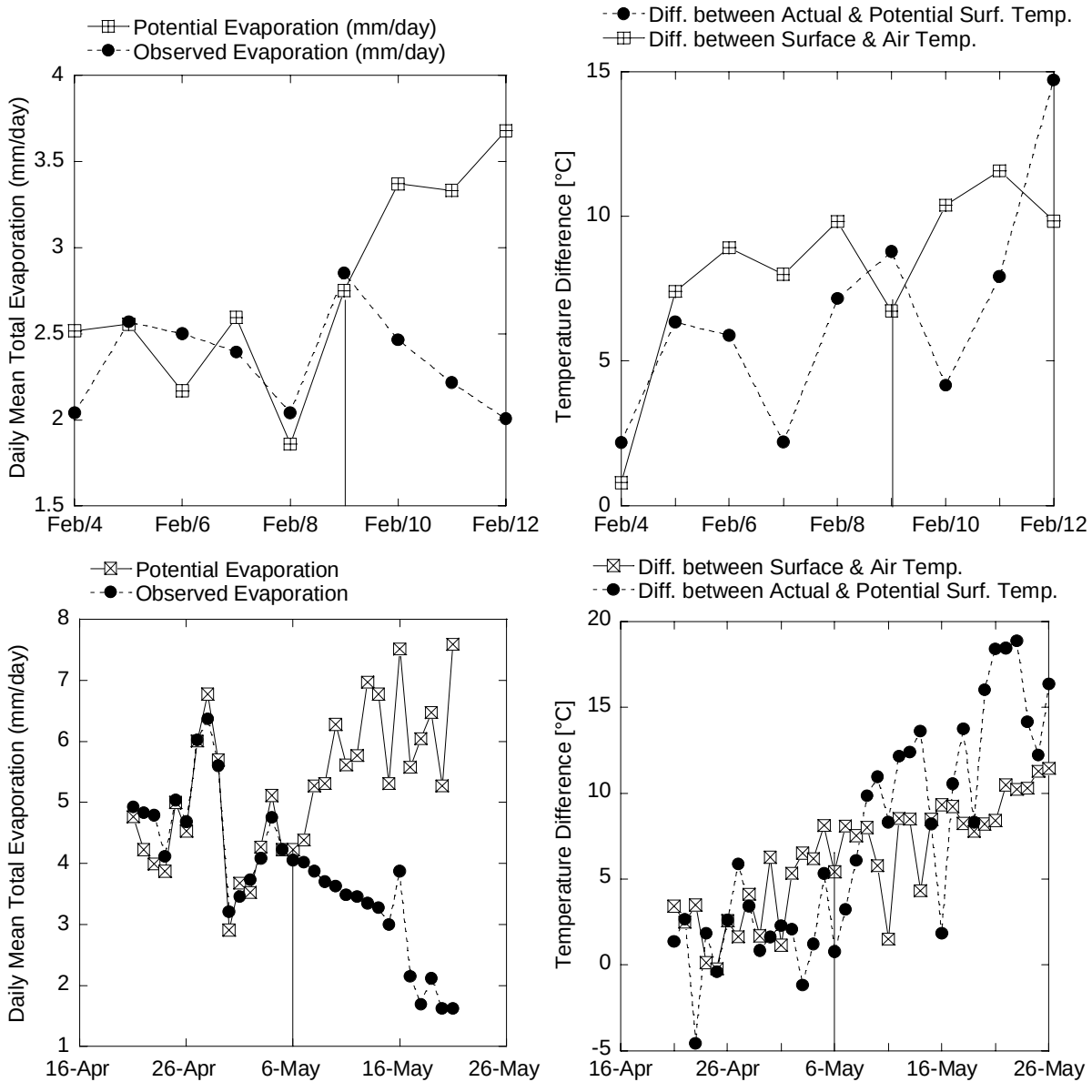
Potential Evaporation (mm/day)
Observed Evaporation (mm/day)
Daily Mean Total Evaporation (mm/day)
Feb/4
Feb/6
Feb/8
Feb/10
Feb/12
Diff. between Actual & Potential Surf. Temp.
Diff. between Surface & Air Temp.
Temperature Difference [°C]
Potential Evaporation
Observed Evaporation
16-Apr
26-Apr
6-May
16-May
26-May
Diff. between Surface & Air Temp.
Diff. between Actual & Potential Surf. Temp.

1 Figure 2

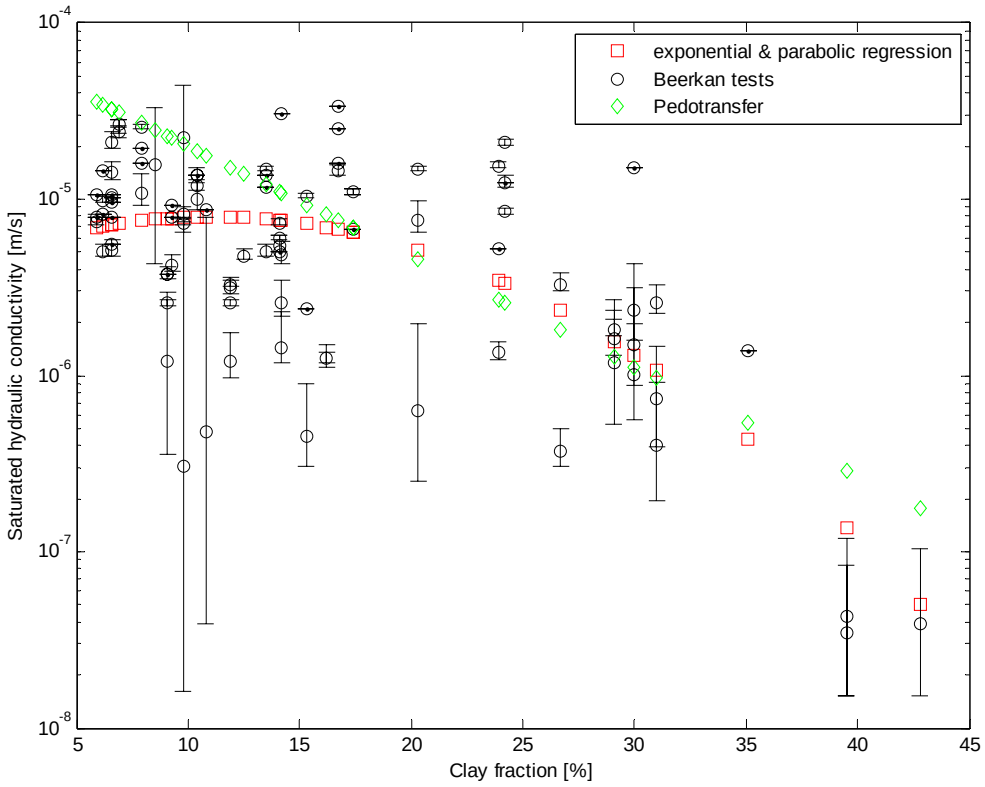
exponential & parabolic regression
Beerkan tests
Pedotransfer
Saturated hydraulic conductivity [m/s]
Clay fraction [%]

2

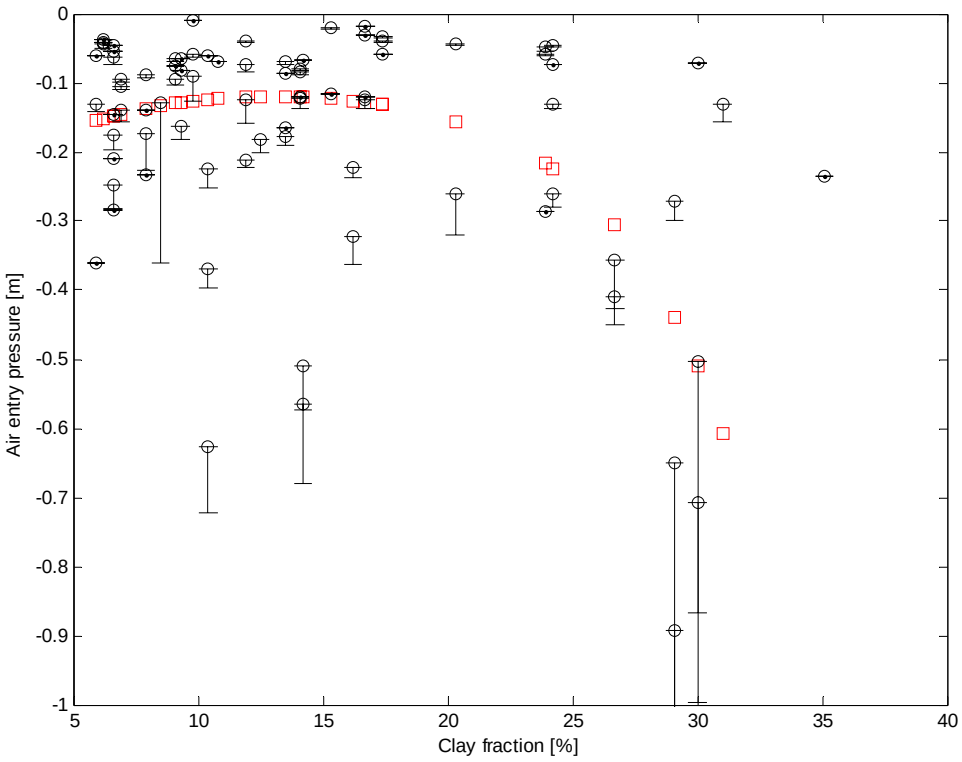
Air entry pressure [m]
Clay fraction [%]

3

1 Figure 3

2

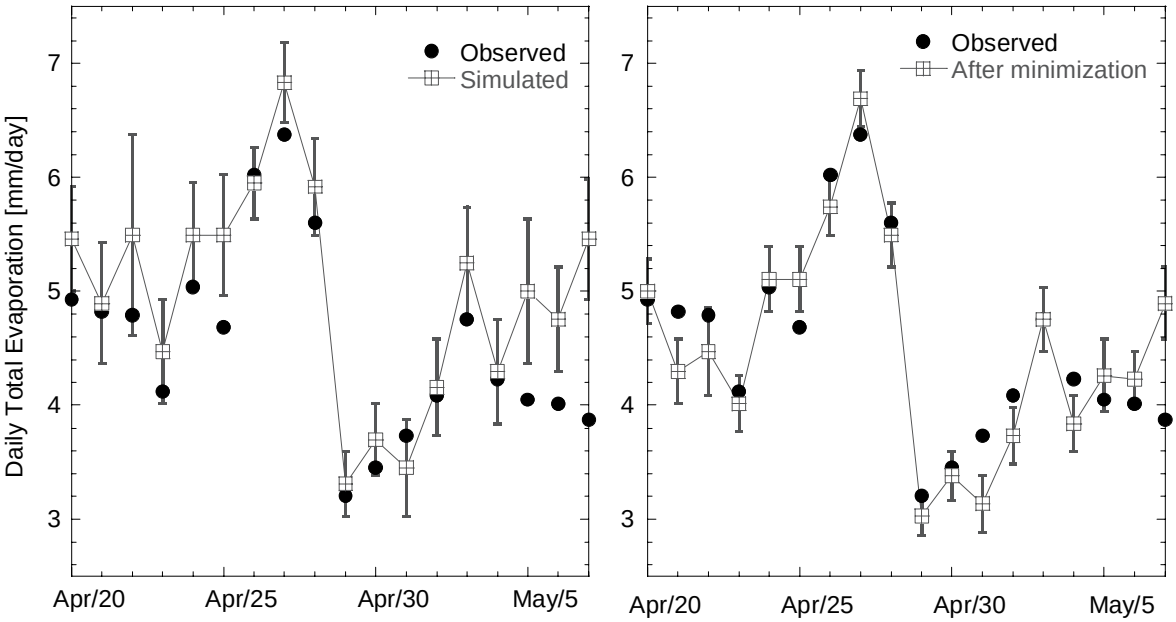
Daily Total Evaporation [mm/day]
Observed
Simulated
Observed
After minimization
Apr/20
Apr/25
Apr/30
May/5
3
4
5
6
7

3

1 Figure 4

2

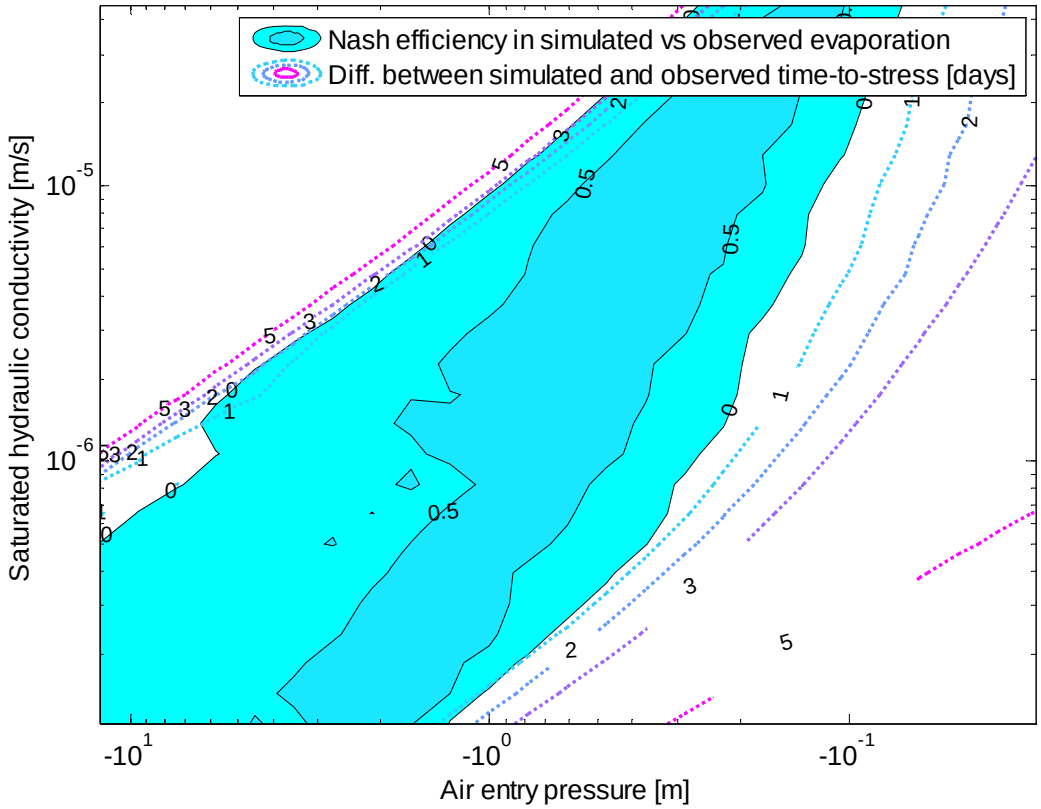
Nash efficiency in simulated vs observed evaporation
Diff. between simulated and observed time-to-stress [days]
Saturated hydraulic conductivity [m/s]
10^-5
10^-6
-10^1
-10^0
-10^-1
Air entry pressure [m]

3

1 Figure 5

2

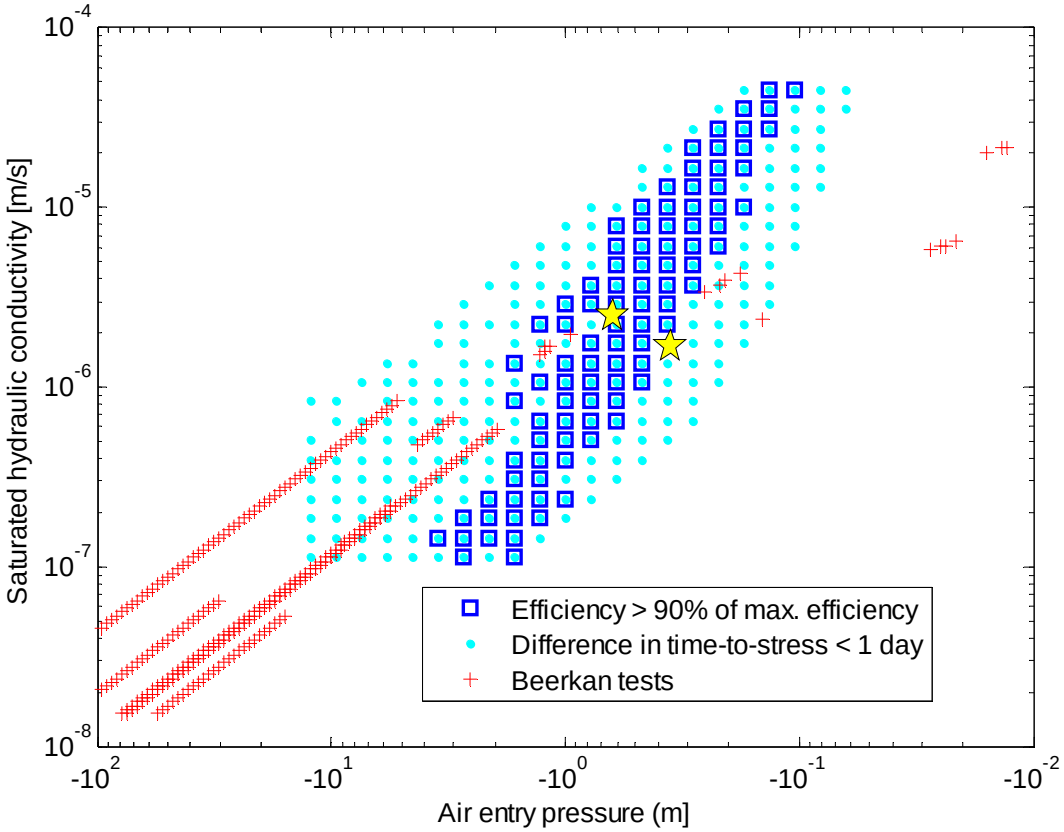
Saturated hydraulic conductivity [m/s]
10^-4
10^-5
10^-6
10^-7
10^-8
-10^2
-10^1
-10^0
-10^-1
-10^-2
Air entry pressure (m)
Efficiency > 90% of max. efficiency
Difference in time-to-stress < 1 day
Beerkan tests

3

1 Figure 6

2

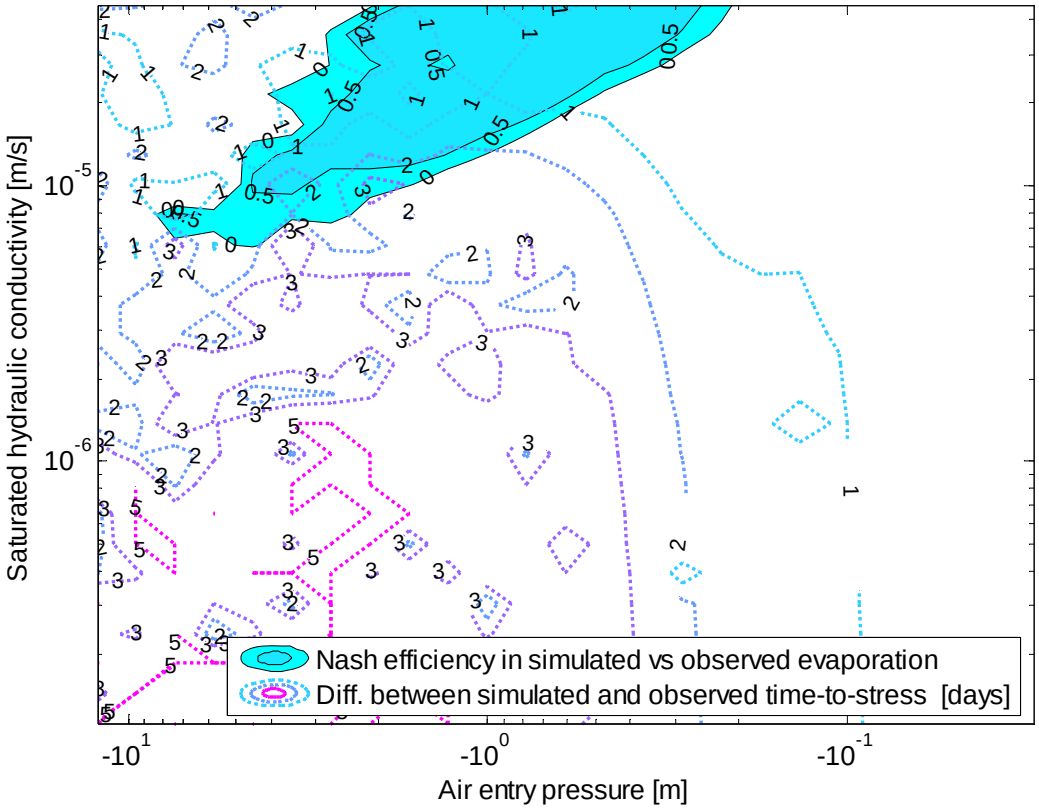
Saturated hydraulic conductivity [m/s]
10^-5
10^-6
-10^1
-10^0
-10^-1
Air entry pressure [m]
Nash efficiency in simulated vs observed evaporation
Diff. between simulated and observed time-to-stress [days]

3

Figure 7

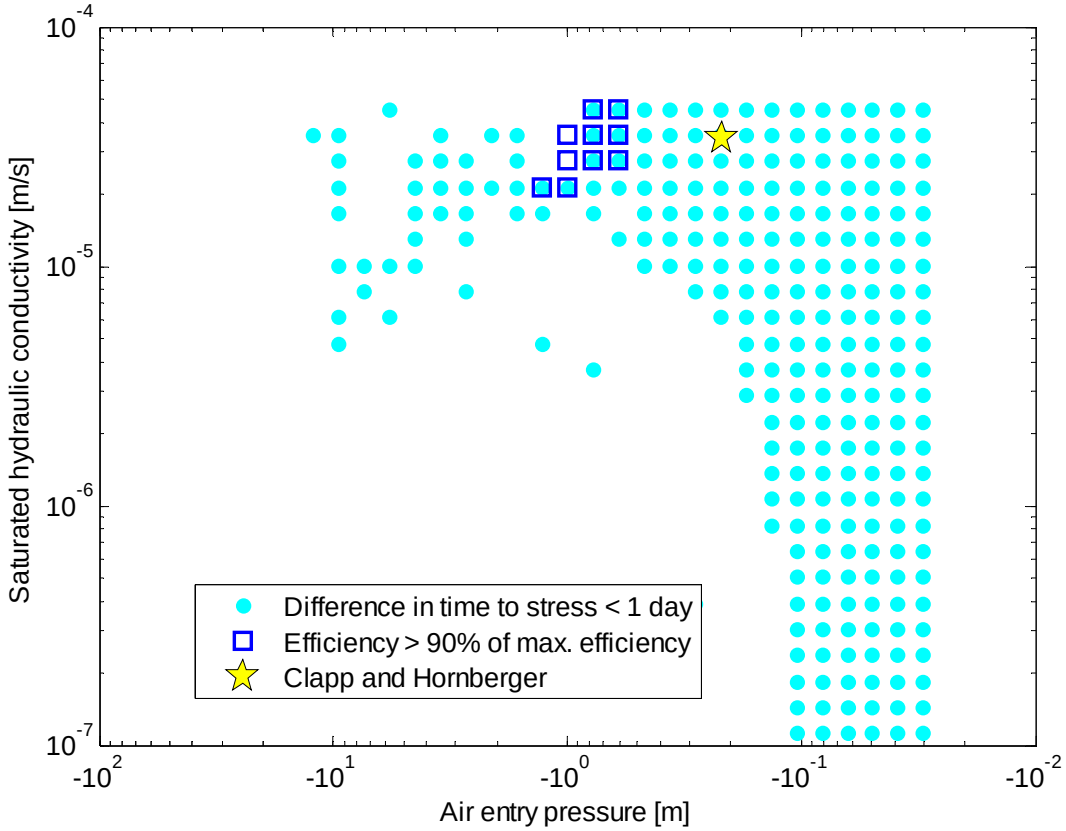
Saturated hydraulic conductivity [m/s]
10^-4
10^-5
10^-6
10^-7
-10^2
-10^1
-10^0
-10^-1
-10^-2
Air entry pressure [m]
Difference in time to stress < 1 day
Efficiency > 90% of max. efficiency
Clapp and Hornberger